Acta Crystallographica Section D
Biological Crystallography
ISSN 1399-0047

Structural and functional analysis of a novel haloalkane dehalogenase with two halide-binding sites

Radka Chaloupkova,[a]‡ Tatyana Prudnikova,[b,c]‡ Pavlina Rezacova,[d,e] Zbynek Prokop,[a] Tana Koudelakova,[a] Lukas Daniel,[a] Jan Brezovsky,[a] Wakako Ikeda-Ohtsubo,[f] Yukari Sato,[f] Michal Kuty,[b,c] Yuji Nagata,[f] Ivana Kuta Smatanova[b,c]* and Jiri Damborsky[a]*

[a]Loschmidt Laboratories, Department of Experimental Biology and Research Centre for Toxic Compounds in the Environment RECETOX, Masaryk University, 625 00 Brno, Czech Republic, [b]Faculty of Science, University of South Bohemia in Ceske Budejovice, Branisovska 31, 370 05 Ceske Budejovice, Czech Republic, [c]Institute of Nanobiology and Structural Biology, Academy of Sciences of the Czech Republic, 142 20 Prague, Czech Republic, [d]Institute of Molecular Genetics, Academy of Sciences of the Czech Republic, 142 20 Prague, Czech Republic, [e]Institute of Organic Chemistry and Biochemistry, Academy of Sciences of the Czech Republic, 166 10 Prague 6, Czech Republic, and [f]Graduate School of Life Sciences, Tohoku University, Sendai 980-8577, Japan

‡ These authors contributed equally to this work.

Correspondence e-mail: ivanaks@seznam.cz, jiri@chemi.muni.cz

Received 7 February 2014
Accepted 21 April 2014

PDB reference: DbeA, 4k2a

The crystal structure of the novel haloalkane dehalogenase DbeA from *Bradyrhizobium elkanii* USDA94 revealed the presence of two chloride ions buried in the protein interior. The first halide-binding site is involved in substrate binding and is present in all structurally characterized haloalkane dehalogenases. The second halide-binding site is unique to DbeA. To elucidate the role of the second halide-binding site in enzyme functionality, a two-point mutant lacking this site was constructed and characterized. These substitutions resulted in a shift in the substrate-specificity class and were accompanied by a decrease in enzyme activity, stability and the elimination of substrate inhibition. The changes in enzyme catalytic activity were attributed to deceleration of the rate-limiting hydrolytic step mediated by the lower basicity of the catalytic histidine.

1. Introduction

Haloalkane dehalogenases (HLDs; EC 3.8.1.5) are microbial enzymes that catalyze the hydrolytic conversion of halogenated aliphatic alkanes and their derivatives into three reaction products: an alcohol, a halide anion and a proton (Chovancová *et al.*, 2007). Structurally, HLDs belong to the superfamily of α/β-hydrolases and consist of a conserved α/β-hydrolase core domain and a helical cap domain (Ollis *et al.*, 1992; Nardini & Dijkstra, 1999; Holmquist, 2000). The active sites of HLDs are buried in a predominantly hydrophobic cavity at the interface between these two domains. The tertiary structures of HLDs have been determined for DhlA from *Xanthobacter autotrophicus* GJ10 (Franken *et al.*, 1991), DhaA from *Rhodococcus rhodochrous* NCIMB 13064 (Newman *et al.*, 1999), LinB from *Sphingobium japonicum* UT26 (Marek *et al.*, 2000), DmbA from *Mycobacterium tuberculosis* H37Rv (Mazumdar *et al.*, 2008), DbjA from *Bradyrhizobium japonicum* USDA110 (Prokop *et al.*, 2010), DppA from *Plesiocystis pacifica* SIR-1 (Hesseler *et al.*, 2011) and DmmA from an unknown marine bacterium (Gehret *et al.*, 2012). The majority of known HLD structures contain a halide anion bound in the active site. This anion is coordinated by the side chains of a highly conserved amino-acid pair, *i.e.* tryptophan–tryptophan (Verschueren, Kingma *et al.*, 1993; Verschueren, Seljée *et al.*, 1993; Pikkemaat *et al.*, 1999; Ridder *et al.*, 1999) or tryptophan–asparagine (Newman *et al.*, 1999; Marek *et al.*, 2000; Oakley *et al.*, 2002, 2004; Streltsov *et al.*, 2003; Monincová *et al.*, 2007; Mazumdar *et al.*, 2008; Prokop *et al.*, 2010). It has been proposed that these two amino acids stabilize the halogen atom of the substrate in the activated complex and the halide anion formed during the dehalogenation reaction (Verschueren, Kingma *et al.*, 1993). The halide-binding site inside the active site of HLDs identified by

protein crystallography has been independently confirmed by site-directed mutagenesis (Krooshof *et al.*, 1998; Bohác *et al.*, 2002), steady-state fluorescence quenching (Verschueren, Kingma *et al.*, 1993), stopped-flow fluorescence (Schanstra *et al.*, 1996; Krooshof *et al.*, 1998; Pikkemaat *et al.*, 1999; Prokop *et al.*, 2003) and steady-state kinetic measurements (Schindler *et al.*, 1999; Prokop *et al.*, 2003).

Besides the two halide-stabilizing residues, the active sites of all HLDs contain three other amino acids essential for catalysis: a nucleophilic aspartate, a basic histidine and a catalytic aspartic or glutamic acid, known together as the catalytic triad (Janssen, 2004; Chovancová *et al.*, 2007). The overall kinetic mechanism of the dehalogenase reaction catalyzed by HLDs proceeds *via* four main steps: (i) substrate binding, (ii) bimolecular nucleophilic substitution resulting in the formation of a halide anion and an alkyl-enzyme intermediate, (iii) nucleophilic addition of a water molecule to the ester intermediate and (iv) release of the reaction products (Verschueren, Seljée *et al.*, 1993; Schanstra *et al.*, 1996; Bosma *et al.*, 2003; Prokop *et al.*, 2003; Silberstein *et al.*, 2007). It has been shown that the rate-limiting step in the catalytic cycle is halide release in the case of DhlA reacting with 1,2-dichloroethane and 1,2-dibromoethane (Schanstra *et al.*, 1996), release of an alcohol and cleavage of the carbon–halogen bond for DhaA with 1,3-dibromopropane (Bosma *et al.*, 2003) and 1,2,3-trichloropropane (Pavlova *et al.*, 2009), and hydrolysis of the alkyl-enzyme intermediate for LinB with 1-chlorohexane, chlorocyclohexane and bromocyclohexane (Prokop *et al.*, 2003). The observed differences in the rate-limiting step suggest that the catalytic efficiency of HLDs is governed by the particular enzyme–substrate pair and depends on: (i) the composition of the catalytic residues, (ii) the geometry and solvation of the enzyme active-site cavity and (iii) the geometry and dynamics of the access tunnels connecting the buried enzyme active site to the surrounding solvent (Pikkemaat *et al.*, 1999; Prokop *et al.*, 2003; Janssen, 2004; Pavlova *et al.*, 2009).

Since the first HLD was isolated in 1985 (Keuning *et al.*, 1985), more than 200 putative HLDs have been identified by phylogenetic analysis and 16 of them have been biochemically characterized (Keuning *et al.*, 1985; Kulakova *et al.*, 1997; Nagata *et al.*, 1999; Jesenská *et al.*, 2002, 2005, 2009; Sato *et al.*, 2005; Chan *et al.*, 2010; Hasan *et al.*, 2011; Hesseler *et al.*, 2011; Drienovska *et al.*, 2012; Gehret *et al.*, 2012). Phylogenetic analysis of HLDs and their putative relatives has revealed that the enzyme family can be divided into three subfamilies, HLD-I, HLD-II and HLD-III, which differ mainly in the composition of the catalytic residues and the anatomy of the cap domain (Chovancová *et al.*, 2007). HLDs are broad substrate-specificity enzymes. Individual members of the HLD family are able to convert a wide spectrum of chlorinated, brominated and iodinated alkanes, alcohols, amides, ethers and esters (Damborský *et al.*, 2001). Systematic exploration of their substrate specificity using a uniform set of halogenated substrates led to the classification of the enzymes into four distinct substrate-specificity groups (Koudelakova *et al.*, 2011). Simultaneous investigation of the relationship between the function and evolution of HLDs showed that it is not possible to predict the substrate specificity of putative HLDs on the basis of sequence similarities with experimentally characterized family members (Koudelakova *et al.*, 2011). Currently recognized structural determinants of HLD substrate specificity are (i) the composition of the catalytic residues, (ii) the size, shape and physicochemical properties of the active-site cavity and (iii) the shape, physicochemical properties and dynamics of the access tunnels (Damborský & Koca, 1999; Marek *et al.*, 2000; Bohác *et al.*, 2002; Otyepka & Damborský, 2002; Kmunícek *et al.*, 2005; Silberstein *et al.*, 2007; Koudelakova *et al.*, 2011).

In the present study, a novel haloalkane dehalogenase, DbeA from *B. elkanii* USDA94, was structurally and biochemically characterized. Crystallographic analysis revealed the presence of two halide-binding sites in the DbeA structure: one in the active site and the second buried in the protein core. The observed spatial proximity of the second halide-binding site to the active-site cavity of DbeA suggests that it may play an important role in enzyme functionality. Detailed insight into the role of the second halide-binding site was obtained by its elimination from the DbeA structure using site-directed mutagenesis. Steady-state kinetics, pre-steady-state kinetics and circular dichroism spectroscopy revealed significant changes in substrate specificity, catalytic activity and stability in the presence of salts.

2. Materials and methods

2.1. Gene isolation, synthesis and cloning

The *dbeA* gene was isolated from *B. elkanii* USDA94 and its nucleotide sequence was deposited in DDBJ/GenBank/EMBL under accession No. AB478942. The C-terminus of the *dbeA* gene was fused to the sequence encoding a hexahistidine tag, enabling purification by metal-affinity chromatography. The recombinant gene *dbeA* ΔCl-His_6 (I44L+Q102H) was synthesized artificially (Entelechon, Regensburg, Germany) according to the wild-type (wt) sequence. The synthesized gene was subcloned into the expression vector pET-21b (Novagen, Madison, USA) using restriction endonucleases *Nde*I and *Xho*I (Fermentas, Burlington, Canada) and T4 DNA ligase (Promega, Madison, USA).

2.2. Protein overexpression and purification

To overproduce DbeA wt and DbeA ΔCl (internal No. DbeA 03) in *Escherichia coli* BL21 (DE3) cells, the corresponding genes were transcribed by T7 RNA polymerase, which is expressed by the isopropyl β-D-1-thiogalactopyranoside (IPTG)-inducible *lac* UV5 promoter. Cells containing these plasmids were cultured in Luria broth medium at 37°C. When the culture reached an optical density of 0.6 at a wavelength of 600 nm, enzyme expression (at 20°C) was induced by the addition of IPTG to a final concentration of 0.5 m*M*. The cells were subsequently harvested and disrupted by sonication using a Soniprep 150 (Sanyo Gallenkamp PLC, Loughborough, England). The supernatant was collected after

centrifugation at 100 000*g* for 1 h. The crude extract was further purified on a HiTrap Chelating HP 5 ml column charged with Ni^{2+} ions (GE Healthcare, Uppsala, Sweden). The His-tagged enzyme was bound to the resin in the presence of equilibration buffer (20 m*M* potassium phosphate buffer pH 7.5, 0.5 *M* sodium chloride, 10 m*M* imidazole). Unbound and nonspecifically bound proteins were washed out by buffer containing 37.5 m*M* imidazole. The target enzyme was eluted with buffer containing 300 m*M* imidazole. The active fractions were pooled and dialyzed against 50 m*M* potassium phosphate buffer pH 7.5 overnight. The enzymes, both of which contained a C-terminal hexahistidyl tail, were stored at 4°C in 50 m*M* potassium phosphate buffer prior to analysis.

2.3. Specific activity measurements

Enzymatic activity towards 30 halogenated substrates was assayed using the colorimetric method developed by Iwasaki *et al.* (1952). The release of halide ions was analyzed spectrophotometrically at 460 nm using a SUNRISE microplate reader (Tecan, Grödig/Salzburg, Austria) after reaction with mercuric thiocyanate and ferric ammonium sulfate. The dehalogenation reaction was performed at 37°C in 25 ml Reacti-flasks with Mininert valves. The reaction mixture contained 10 ml glycine buffer (100 m*M*, pH 8.6) and 10 µl of an appropriate halogenated substrate at a concentration of 0.1–10 m*M* depending on the substrate solubility. The reaction was initiated by the addition of enzyme. The reaction was monitored by withdrawing 1 ml samples at periodic intervals from the reaction mixture and immediate mixing of the samples with 0.1 ml 35% nitric acid to terminate the reaction. Dehalogenation activity was quantified as the rate of product formation with time.

2.4. Principal component analysis

A matrix containing the activity data for nine wt HLDs and one mutant HLD with 30 substrates was analyzed by principal component analysis (PCA; Wold *et al.*, 1987). The aim of the analysis was to uncover relationships between individual HLDs based on their activities towards the set of substrates (Koudelakova *et al.*, 2011). In brief, two PCAs were performed using *Statistica* 9.0 (StatSoft, Tulsa, USA). In the first analysis, raw data of the specific activities were used as the primary input data. This analysis compared the overall activity of the mutant enzyme with the overall activity of wt HLDs. In the second analysis, the raw data were log-transformed and weighted relative to the activity of the the individual enzyme towards other substrates prior to performing the PCA in order to better discern the enzyme specificity profiles (Koudelakova *et al.*, 2011). These transformed data were used to identify substrate-specificity groups of enzymes that exhibited similar specificity profiles regardless of their overall specific activities.

2.5. Steady-state kinetic measurements

The catalytic properties of the enzymes were described by steady-state kinetic parameters determined with selected substrates. Steady-state kinetic constants for the reaction between DbeA wt and 1-chlorobutane or 1,3-dibromopropane were evaluated by measuring the substrate and product concentrations using a Trace GC 2000 gas chromatograph (Finnigen, San Jose, USA) equipped with a flame ionization detector and a DB-FFAP 30 m × 0.25 mm × 0.25 µm capillary column (J&W Scientific, Folsom, USA) and the colorimetric method described by Iwasaki *et al.* (1952), respectively. Dehalogenation was performed at 37°C in 25 ml Reacti-flasks with Mininert valves in a shaking water bath. The reaction mixture consisted of 10 ml glycine buffer (100 m*M*, pH 8.6) and various concentrations of substrate (0.01–5 m*M* for 1-chlorobutane and 0.01–7 m*M* for 1,3-dibromopropane). The enzymatic reaction was initiated by the addition of DbeA wt to final concentrations of 2.09 and 0.14 µ*M* for the reactions with 1-chlorobutane and 1,3-dibromopropane, respectively. The reaction was terminated by the addition of 0.1 ml 35% nitric acid at different times after initiation (0, 10, 20, 30 and 40 min). All data points corresponded to the mean of three independent replicates. Kinetic parameters were determined by nonlinear curve-fitting the data points using the *Origin* 6.1 software (OriginLab, Massachusetts, USA). The steady-state kinetics of DbeA wt and DbeA ΔCl with 1-bromobutane were measured using a VP-ITC isothermal titration microcalorimeter (MicroCal, Piscataway, USA). The substrate was dissolved in 100 m*M* glycine buffer pH 8.6 and the solution was allowed to reach thermal equilibrium in the reaction cell (1.4 ml). The reaction was initiated by injecting 10 µl enzyme solution containing either 26 µ*M* DbeA wt or 825 µ*M* DbeA ΔCl into the reaction cell. The enzymes were dialyzed overnight against the same glycine buffer as was used to dissolve the substrate. The measured rate of heat change was assumed to be directly proportional to the velocity of the enzymatic reaction according to

$$\frac{dQ}{dt} = -\Delta H V \frac{d[S]}{dt}, \qquad (1)$$

where ΔH is the enthalpy of the reaction, $[S]$ is the substrate concentration and V is the volume of the cell. ΔH was determined by titrating the substrate into the reaction cell containing the enzyme. Each reaction was allowed to proceed to completion. The integrated total heat of reaction was divided by the amount of injected substrate. The evaluated rate of substrate depletion ($-d[S]/dt$) and the corresponding substrate concentrations were then fitted by nonlinear regression to kinetic models using *Origin* 6.1 (OriginLab, Massachusetts, USA).

2.6. Size-exclusion chromatography

The molecular weight of DbeA wt was analyzed using an ÄKTA FPLC system equipped with UV_{280} detection (GE Healthcare, Uppsala, Sweden) and a Superdex 200 10/300 GL column (GE Healthcare, Uppsala, Sweden). A total volume of 100 µl of the protein sample was applied onto the column and separated at a constant flow rate of 0.5 ml min^{-1}. The elution buffer comprised 50 m*M* Tris–HCl and 150 m*M* NaCl. For calibration against molecular-weight standards, a gel-filtration calibration kit (GE Healthcare, Uppsala, Sweden) was used

containing ribonuclease A (13.7 kDa), chymotrypsinogen A (25 kDa), ovalbumin (43.0 kDa), conalbumin (75.0 kDa) and aldolase (158 kDa). All molecular-weight standards, as well as protein samples, were dialyzed against the elution buffer prior to analysis.

2.7. Native gel electrophoresis

The oligomeric state of DbeA wt was also investigated by native polyacrylamide gel electrophoresis performed with 10% gels lacking sodium dodecyl sulfate. The electrophoresis tank was maintained at 4°C during the experiment. The gels were stained with Coomassie Brilliant Blue R-250 dye (Fluka, Buchs, Switzerland). The molecular mass of DbeA wt was estimated by comparison of its mobility with the values for two molecular-weight standards, ovalbumin (43.0 kDa) and albumin (67.0 kDa), and three HLDs, DhaA (33.2 kDa), LinB (33.1 kDa) and DmbA (33.7 kDa).

2.8. Circular dichroism spectroscopy and thermal denaturation

To assess the secondary structure and correct folding of the enzymes, circular dichroism (CD) spectra were recorded at room temperature using a Jasco J-810 spectropolarimeter (Jasco, Tokyo, Japan). Data were collected from 185 to 260 nm (in pure 50 m*M* phosphate buffer pH 7.5) or from 200 to 260 nm (in the presence of sodium chloride) at a scan rate of 100 nm min^{-1} with a 1 s response time and a 2 nm bandwidth using a 0.1 cm quartz cuvette containing the enzyme. Each spectrum shown represents an average of ten individual scans and has been corrected for absorbance caused by the buffer. CD data were expressed in terms of the mean residue ellipticity ($\Theta_{\rm MRE}$). Thermal unfolding of the studied enzymes was followed by monitoring the ellipticity at 222 nm over a temperature range of 20–80°C using a resolution of 0.1°C and a heating rate of 1°C min^{-1}. The resulting thermal denaturation curves were roughly normalized to represent a signal change between approximately 1 and 0 and were fitted to sigmoidal curves using *Origin* 6.1 (OriginLab, Massachusetts, USA). The melting temperature ($T_{\rm m}$) was evaluated as the midpoint of the normalized thermal transition.

2.9. Crystallization and data collection

DbeA wt was crystallized by the sitting-drop vapour-diffusion procedure from a solution consisting of 100 m*M* Tris–HCl pH 7.5, 20%(*w*/*v*) PEG 3350 or 4000, 150 m*M* calcium acetate as described previously by Prudnikova *et al.* (2009). Diffraction data were collected on MX14.2 operated by the Helmholtz-Zentrum Berlin (HZB) at the BESSY II electron-storage ring (Berlin-Adlershof, Germany; Mueller *et al.*, 2012) with a 0.918 Å monochromatic fixed wavelength. The data were processed using the *HKL*-3000 package (Minor *et al.*, 2006). The crystals exhibited the symmetry of space group $P2_12_12_1$ and contained four molecules in the asymmetric unit, with a solvent content of ∼50%. The crystals exhibited anisotropic diffraction; the low value of the completeness and the high value of $I/\sigma(I)$ in the highest resolution shell are a consequence of this anisotropy. Crystal parameters and data-collection statistics are given in Table 1.

Table 1
Diffraction data-collection and refinement statistics.

Values in parentheses are for the highest resolution shell.

X-ray diffraction data-collection statistics	
Space group	$P2_12_12_1$
Unit-cell parameters (Å, °)	a = 62.7, b = 121.9, c = 161.9, $\alpha = \beta = \gamma$ = 90
No. of molecules in asymmetric unit	4
Wavelength (Å)	0.918
Resolution (Å)	2.2
No. of unique reflections	63890
Multiplicity	5.8 (3.4)
Completeness (%)	92.3 (62.8)
$R_{\rm merge}$† (%)	6.6 (24.8)
Average $I/\sigma(I)$	25.0 (4.3)
Wilson B (Å^2)	25.672
Refinement statistics	
Resolution range (Å)	50–2.2 (2.28–2.20)
No. of reflections in working set	55927 (2690)
R‡ (%)	14.53
$R_{\rm free}$§ (%)	20.66
R.m.s.d., bond lengths (Å)	0.013
R.m.s.d., angles (°)	1.592
Contents of asymmetric unit	
Total No. of atoms	9983
No. of protein atoms	9222
No. of water molecules	749
No. of acetate ions	3
No. of chloride ions	8
Mean B values (Å^2)	
Protein	23.98
Ion Cl1	22.28
Ion Cl2	24.06
Ramachandran plot statistics (%)	
Residues in favoured regions	95.16 [1144/1203]
Residues in allowed regions	96.13 [1156/1203]
PDB code	4k2a

† $R_{\rm merge} = \sum_{hkl}\sum_i |I_i(hkl) - \langle I(hkl)\rangle| / \sum_{hkl}\sum_i I_i(hkl)$, where $I_i(hkl)$ is an individual intensity of the ith observation of reflection hkl and $\langle I(hkl)\rangle$ is the average intensity of reflection hkl with summation over all data. ‡ $R = \sum_{hkl} ||F_{\rm obs}| - |F_{\rm calc}|| / \sum_{hkl} |F_{\rm obs}|$, where $F_{\rm obs}$ and $F_{\rm calc}$ are the observed and the calculated structure factors, respectively. § $R_{\rm free}$ is equivalent to R but is calculated using 5% of the reflections that were chosen at random and omitted from the refinement process.

2.10. Structure determination and refinement

The structure of DbeA wt was solved by the molecular-replacement method using *MOLREP* (Vagin & Teplyakov, 2010) with the structure of DhaA from *Rhodococcus* sp. (PDB entry 1bn6; Newman *et al.*, 1999) as a search model. Model refinement was carried out using *REFMAC* 5.2 (Murshudov *et al.*, 2011) from the *CCP*4 package (Winn *et al.*, 2011) interspersed with manual adjustments using *Coot* 0.5 (Emsley & Cowtan, 2004). The final steps included translation–libration–screw (TLS) refinement (Winn *et al.*, 2001). The refinement statistics are given in Table 1. The following services were used to analyze the structures: *MolProbity* (Chen *et al.*, 2010), the *PISA* server (Krissinel & Henrick, 2005, 2007) and the *Protein–Protein Interaction Server* (Jones & Thornton, 1996). Figures showing structural representations were prepared using *PyMOL* (Schrödinger). Atomic coordinates and experimental structure factors have been deposited in the Worldwide Protein Data Bank under PDB code 4k2a.

2.11. Pre-steady-state kinetic measurements

To identify the rate-determining step for the catalytic conversion of 1-bromobutane by the enzymes, rapid-quench flow experiments were performed at 37°C in glycine buffer at pH 8.6 using a model QFM 400 instrument (Bio-Logic, Claix, France). The reaction was initiated by rapid mixing of 70 µl enzyme solution with 70 µl substrate solution and was quenched with 100 µl 0.8 *M* H_2SO_4 at times ranging from 2 ms to 1.2 s. The quenched mixture was directly injected into 0.5 ml ice-cold diethyl ether containing 1,2-dichloroethane as an internal standard. After extraction, the diethyl ether layer containing noncovalently bound substrate and alcohol product was collected, dried on a short column packed with anhydrous Na_2SO_4 and analyzed using a Trace 2000 gas chromatograph equipped with MS detection (Finnigen, San Jose, USA) and a DB-5MS capillary column (J&W Scientific, Folsom, USA). The amount of bromide ion in the aqueous phase was measured by ion chromatography using an 861 Advanced Compact IC equipped with a METROSEP A Supp 5 column (Metrohm, Herisau, Switzerland).

Stopped-flow fluorescence experiments were used to study the kinetics of halide binding to the enzymes. Binding experiments were performed using a SFM-20 stopped-flow instrument (Bio-Logic, Claix, France) combined with a Jasco J-810 spectropolarimeter (Jasco, Tokyo, Japan) equipped with an Xe arc lamp with excitation at 295 nm and a SFM-300 stopped-flow instrument combined with a MOS-200 spectrometer (Bio-Logic, Claix, France). Fluorescence emission from tryptophan residues was observed through a 320 nm cutoff filter upon excitation at 295 nm. Reactions were performed at 37°C in glycine buffer at pH 8.6. Dissociation constants were calculated from the amplitudes of fluorescence quenching for the rapid equilibrium phase. Amplitudes and observed rate constants for the slow kinetic phase were evaluated by fitting to single exponentials using *Origin* 6.1 (OriginLab, Massachusetts, USA).

2.12. Calculation of binding energies

Molecular-dynamics (MD) simulations were used to analyze the binding energies of ions to their respective binding sites. The crystal structure of DbeA wt was employed as a starting model, while the double mutant DbeA ΔCl (I44L+Q102H) was constructed in *PyMOL* (Schrödinger). The orientation of the introduced side chains was chosen to be the same as in the aligned structure of the haloalkane dehalogenase LinB (PDB entry 1mj5), which naturally contains the target residues. H atoms were added to the structure of DbeA wt and DbeA ΔCl with the *H*++ server at pH 7.5 (Gordon *et al.*, 2005). A chloride ion was placed at the second halide-binding site of DbeA ΔCl based on its position in the crystal structure of DbeA wt. All water molecules present in the initial crystal structure were retained in both systems. Cl^- and Na^+ ions were added to a concentration of 0.1 *M* using the *tleap* module of *Amber*11 (Case *et al.*, 2010). Using the same module, an octahedral box of TIP3P water molecules (Jorgensen *et al.*, 1983) was also added that extended to a distance of 10 Å from any solute atom in the system.

The systems were minimized in five rounds consisting of 250 steepest-descent steps and 750 conjugate-gradient steps with a decreasing restraint on the protein backbone (500, 125, 50, 25 and 0 kcal mol^{-1} $Å^{-2}$). Subsequent MD simulations employed periodic boundary conditions, the particle mesh Ewald method for treatment of electrostatic interactions (Darden *et al.*, 1993), a 10 Å cutoff for nonbonded interactions and a 2 fs time step coupled with the *SHAKE* algorithm (Ryckaert *et al.*, 1977) to fix all bonds that involved hydrogen. Equilibration simulations consisted of two steps: (i) 20 ps of gradual heating from 0 to 310 K under constant volume using a Langevin thermostat with a collision frequency of 1.0 ps^{-1} and harmonic restraints of 5.0 kcal mol^{-1} $Å^{-2}$ on the position of all protein and ligand atoms and (ii) 2000 ps of unrestrained MD simulation at 310 K using the Langevin thermostat, a constant pressure of 100 kPa and a pressure coupling constant of 1.0 ps. Finally, production MD simulations were run for 20 ns with the same settings as the second step of the equilibration MD simulations. Coordinates were saved at 1 ps intervals. The resulting trajectories were analyzed using the *ptraj* module of *Amber*11 and visualized in *PyMOL* v.1.5 and *VMD* v.1.9.1 (Humphrey *et al.*, 1996). All calculations were carried out in the *PMEMD* module of *Amber*11 using the ff10 force field (Hornak *et al.*, 2006). A total of four independent MD simulations were run for each system.

Binding energies were calculated from the trajectories using the molecular mechanics/generalized Born surface area method (Still *et al.*, 1990; Onufriev *et al.*, 2004). Every tenth frame in the last 15 ns of each trajectory was selected for analysis. Energy differences were calculated by combining the gas-phase energy contributions with solvation free-energy components obtained using the implicit solvent model for each species. Input topologies of receptors, ligands and receptor–ligand complexes were prepared with the *leap* module of *Amber*11 using the ff10 force field. The following settings were used for the calculation: PBradii were set to mbondi2, generalized Born model = 5 and saltcon = 0.1 *M* (Onufriev *et al.*, 2004). The analysis was performed with the python script `MMPBSA.py` implemented in *AmberTools*11 (Case *et al.*, 2010).

2.13. Computational prediction of pK_a

The pK_a of the catalytic base in DbeA wt and DbeA ΔCl was calculated from MD simulations. The input file controlling the simulation was generated by the *AmberTools*12 script `cpinutil.py` with the flag for the generalized Born model set to 5. The systems were minimized in five rounds consisting of 250 steepest-descent steps and 750 conjugate-gradient steps with a decreasing restraint on the protein backbone (500, 125, 50, 25 and 0 kcal $mol^{-1}Å^{-2}$). The settings used for all subsequent implicit solvent MD simulations were as follows: interior dielectric constant = 1, saltcon = 0.1 *M*, nonbonded cutoff = 999 and generalized Born model = 5. The particle mesh Ewald method was used to treat electrostatic inter-

actions and a 2 fs time step coupled with the *SHAKE* algorithm was used to fix all bonds involving H atoms. Equilibration simulations consisted of two steps: (i) 20 ps of gradual heating from 0 to 310 K and (ii) 5 ns of MD simulation at 310 K. During both steps, the Langevin thermostat with a collision frequency of 10 ps^{-1} was used to control the temperature and harmonic restraints of 1.0 kcal mol^{-1} $Å^{-2}$ were applied to the positions of the protein backbone atoms and chloride ion. Finally, a 15 ns constant pH MD simulation (Mongan *et al.*, 2004) was run for the whole system with the positions of the atoms in the protein backbone and chloride ion restrained by 0.1 kcal mol^{-1} $Å^{-2}$. The pH of the solvent was set to 8.6 and a period of ten steps was used between Monte Carlo sampling of the protonation state. Coordinates were saved every 1 ps. All calculations were carried out in the *sander* module of *Amber*11 using the constph force field (a modified ff10 force field). A total of two independent MD simulations were run for each system.

3. Results

3.1. Isolation and biochemical characterization of the novel haloalkane dehalogenase DbeA

An open reading frame encoding a putative HLD, designated *dbeA*, was identified in the genome of *B. elkanii* USDA94 by comparing sequences of known HLDs with sequences deposited in genetic databases. The *dbeA* gene was subcloned into pET-21b, overexpressed in *E. coli* BL21 (DE3) and the His-tagged protein was purified to homogeneity with a yield of 40 mg per litre of cell culture. The specific activity of purified DbeA was tested against a set of 30 different halogenated aliphatic substrates representing a wide range of structures and physicochemical properties (Koudelakova *et al.*, 2011). DbeA generally exhibited high activity towards terminally substituted iodinated and brominated compounds but poor activity towards chlorinated compounds (Supplementary Table S1[1]). The optimal alkyl-chain length of the substrate catalyzed by DbeA was between three and four C atoms. The highest enzyme activity (0.0926 µmol s^{-1} mg^{-1}) was observed in the reaction with 1,3-diiodopropane. Principal component analysis revealed that the level of DbeA activity was moderate compared with other HLDs and classified DbeA into substrate-specificity group IV (SSG-IV), the members of which (including DatA and DmbC) preferentially convert terminally brominated and iodinated propanes and butanes (Koudelakova *et al.*, 2011).

The catalytic properties of DbeA were assessed by measuring steady-state kinetic constants with 1-chlorobutane, 1-bromobutane and 1,3-dibromopropane as substrates (Supplementary Table S2). DbeA kinetics with 1-chlorobutane followed a simple hyperbolic Michaelis–Menten relationship. Surprisingly, changing the substituent in the substrate from chlorine to bromine resulted in sigmoidal kinetics accompanied by weak substrate inhibition in the reaction with 1-bromobutane. This suggests that DbeA is able to accommodate 1-bromobutane inside the catalytic pocket better than 1-chlorobutane and that binding of 1-bromobutane in the enzyme pocket occurs in a cooperative manner. Examination of the kinetics of DbeA towards 1,3-dibromopropane revealed another interesting feature, *i.e.* strong substrate inhibition with $K_{si} < K_m$ combined with a cooperative mechanism. These results indicate that the mechanism by which DbeA catalyzes conversion of halogenated compounds is strongly dependent on the specific halogen and chemical structure of the substrate.

The size, secondary structure and thermostability of DbeA were also investigated. Gel-filtration chromatography (Supplementary Fig. S1*a*) and native gel electrophoresis (Supplementary Fig. S1*b*) were employed for determination of the oligomeric state of DbeA. DbeA was found to exist as a dimer in solution under the tested conditions. CD spectroscopy was used to investigate the correct folding and thermostability of DbeA. Far-UV CD spectra of DbeA and other related HLDs (Supplementary Fig. S2) exhibited one positive peak at 195 nm and two negative features at 222 and 208 nm, characteristic of α-helical content (Fasman, 1996) and implying correct folding of DbeA. Thermally induced denaturation of DbeA indicated a melting temperature of T_m = 58.5 ± 0.2°C (Supplementary Table S3).

3.2. Structural characterization of DbeA and identification of two halide-binding sites

The crystal structure of DbeA was solved by protein crystallography to 2.2 Å resolution (Table 1). The domain organization of DbeA was found to be very similar to those of other structurally known HLD enzymes. Two distinct domains, the α/β-hydrolase core domain and α-helical cap domain, are separated by a deep cleft (Fig. 1). The core domain consists of a central eight-stranded β-sheet with β2 lying in an antiparallel orientation with respect to the direction of the β-sheet. The β-sheet is flanked by five α-helices on both sides. The cap

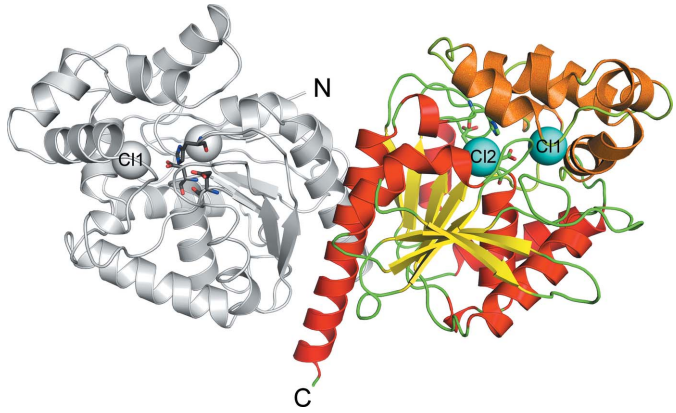

Figure 1
Overall structure of DbeA. C^{α} ribbon trace representing the elements of the protein secondary structure. α-Helices are shown in red for the main domain and in orange for the cap domain; β-strands are shown in yellow; loops are shown in green; chloride ions are shown as cyan spheres; the chloride ion in the canonical product-binding site is labelled Cl1; the chloride ion bound in the second halide-binding site is labelled Cl2; the catalytic triad residues are shown as sticks.

[1] Supporting information has been deposited in the IUCr electronic archive (Reference: DW5094).

domain protecting the upper surface of the active-site cavity consists of six short α-helices linked by seven loop insertions. Similar to other HLDs, DbeA contains five catalytic residues in the active site: the nucleophile Asp103, the catalytic base His271 and the catalytic acid Glu127, forming the so-called catalytic triad, and two-halide stabilizing residues Asn38 and Trp104. Analysis of the intermolecular contacts in the crystal structure suggested that DbeA dimerization is mediated through the interaction of the C-terminal α-helices formed by residues 273–303 (Fig. 1).

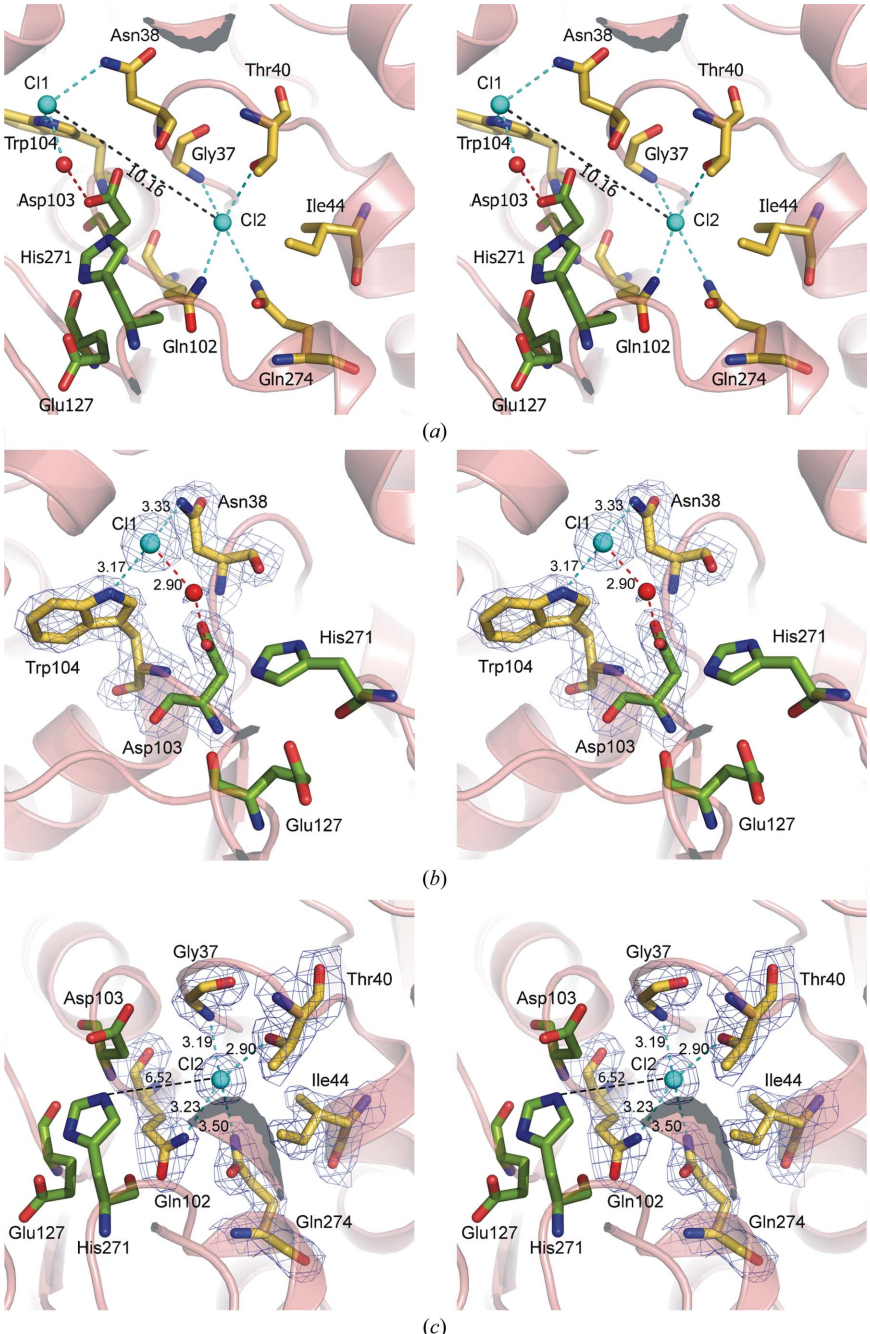

Figure 2
Active site of DbeA (stereoview). (*a*) Overview of the active site with two chloride ions. Residues coordinating the chloride ions are represented by sticks with C atoms shown in yellow; the C atoms of the catalytic triad are shown in green. Two chloride ions are shown as cyan spheres with coordinating interactions represented by cyan dashed lines. A water molecule and water-mediated interactions are shown in red; the distance between the two chloride ions is indicated by the number (in Å) over the black dashed line. (*b*) Expanded view of a chloride ion in the canonical halide-binding region (Cl1) of the active site. The $2F_o - F_c$ electron-density map for ions and interacting residues contoured at 1.5σ is shown in blue; the numbers indicate the coordination distances (in Å). (*c*) Expanded view of a chloride ion bound to the unique second halide-binding site (Cl2). The distance between the catalytic histidine and the chloride anion is indicated by the number (in Å) over the black dashed line.

During refinement of the crystal structure, two peaks in the electron density were detected indicating the presence of two ions in the vicinity of the DbeA active site. Since sodium chloride was the only halide-containing compound used in purification and crystallization, two chloride anions were modelled in the electron density, both with an occupancy of 1.0 in all four molecules accommodated in one asymmetric unit. The position of the two chloride anions and coordinating amino-acid residues are shown in Fig. 2(*a*). The identity of the ions was corroborated by the presence of strong peaks in an anomalous difference map calculated from diffraction data collected at wavelength 1.5 Å. The first chloride anion (designated as Cl1) in the DbeA structure occupies the product-binding site and interacts with N atoms from the conserved halide-binding residues Asn38 $N^{\delta2}$ and Trp104 $N^{\varepsilon1}$, with distances of 3.33 and 3.17 Å, respectively (Fig. 2*b*). Further coordination is provided by a water molecule mediating contact with the side chain of the catalytic residue Asp103. The distance between the water molecule O atom and the chloride ion Cl1 is 3.33 Å. This halide-binding site is common to all members of the HLD family (Janssen, 2004; Damborsky *et al.*, 2010). The second chloride anion (designated Cl2) is located about 10 Å from the product-binding site and is buried deep in the protein core. It is coordinated by the side-chain atoms of Gln274 $N^{\delta2}$, Gln102 $N^{\delta2}$, Gly37 N and Thr40 $O^{\gamma1}$ and is positioned 3.50, 3.23, 3.19 and 2.90 Å away, respectively (Fig. 2*c*). This second halide-binding site is unique to DbeA and has not previously been observed in any other crystal structure of a related HLD. The full occupancy of this second halide-binding site and its location in close proximity ($\sim$ 10 Å, Fig. 2*a*) to the active site suggest that it might have biological relevance.

Chloride binding to DbeA wt in solution was monitored by stopped-flow fluorescence, revealing two distinct phases: a rapid equilibrium phase followed by a slow exponential phase (Fig. 3*a*). The first phase reached rapid equilibrium within the dead

time of the instrument (0.5–5.0 ms), and therefore a difference in the initial fluorescence signal was only observed after mixing DbeA wt with increasing concentrations of halides. The second kinetic phase was characterized by a single exponential decrease of the fluorescence signal with time. The chloride concentration dependence of the amplitudes of the initial and kinetic exponential phase (Figs. 3*c* and 3*e*) indicated the presence of two independent binding sites for chloride ions in the enzyme with derived dissociation constants for the fast and the slow binding interactions of $K_{d1} = 0.10 \pm 0.05$ *M* and $K_{d2} = 0.37 \pm 0.06$ *M*, respectively. The observed rate constants for the second kinetic phase showed a linear dependence on chloride concentration (Fig. 3*f*), indicating that the slow kinetic phase is associated with chloride binding. The kinetic data were fitted to a linear equation, yielding an association rate constant ($6.1 \pm 0.9\ M^{-1}\ s^{-1}$) and dissociation rate constant ($5.3 \pm 1.0\ s^{-1}$) for binding of chloride to the second halide-binding site. Similar results were observed when bromide binding to DbeA wt was monitored by stopped-flow fluorescence (Supplementary Fig. S3). Previous studies investigating the binding of halide ions to haloalkane dehalogenases revealed the presence of a single halide-binding site in DhlA (Schanstra *et al.*, 1996), LinB (Prokop *et al.*, 2003) and DatA (Hasan *et al.*, 2013).

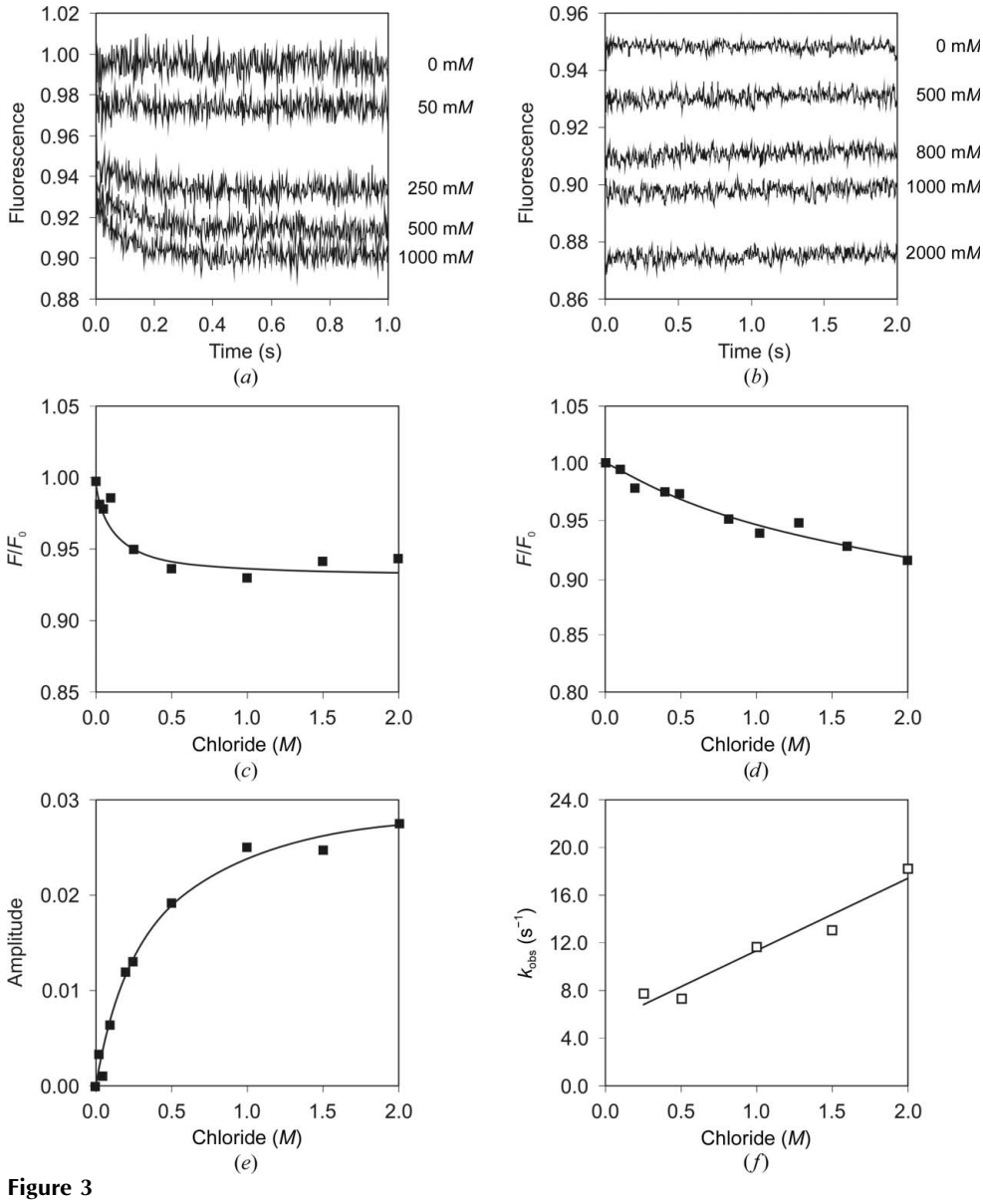

Figure 3
Stopped-flow fluorescence analysis of chloride binding to DbeA wt and DbeA ΔCl. (*a*) Fluorescence traces obtained upon mixing 30 μ*M* DbeA wt with chloride. (*b*) Fluorescence traces obtained upon mixing 30 μ*M* DbeA ΔCl with chloride. (*c*) Chloride concentration dependence of rapid equilibrium fluorescence quench of DbeA wt. (*d*) Chloride concentration dependence of rapid equilibrium fluorescence quench of DbeA ΔCl. (*e*) Chloride dependence of the amplitude of the slow exponential fluorescence quench of DbeA wt. Solid lines represent best fits to the data based on the Stern–Volmer equation $F/F_0 = \{1 + (fK_q[Cl^-])\}/(1 + K_{Cl}[Cl^-])$, in which F/F_0 is the relative fluorescence, f is the relative fluorescence intensity of the enzyme–chloride complex, K_{Cl} is the association equilibrium constant of specific binding of chloride and K_q is the quenching constant, which is the apparent association equilibrium constant of the nonspecific quenching interaction between chloride and the fluorophore. (*f*) Chloride dependence of the observed rate constants of the slow exponential fluorescence quench of DbeA wt. The solid line represents the best fit to the data using the equation $k_{obs} = k_{assoc}[Cl^-]/k_{dissoc}$, where k_{assoc} and k_{dissoc} are the association and dissociation rate constants, respectively.

3.3. Construction of the variant DbeA ΔCl with an eliminated second halide-binding site

Comparison of the structure and amino-acid sequence of DbeA with those of other related enzymes revealed that the second halide-binding side is lined by five amino-acid residues: Gly37, Thr40, Ile44, Gln102 and Gln274 (Fig. 4). Ile44 and Gln102 are unique to DbeA and their substitution by Leu and His residues, as found in other HLDs, reduced the volume of the second halide-binding site by 10%. The two-point mutant I44L+Q102H (designated DbeA ΔCl) was constructed and characterized to gain a deeper understanding of the role of the second halide-binding site in determining the structure and function of DbeA.

Since attempts to crystallize DbeA ΔCl were not successful, disruption of the second halide-binding site in DbeA ΔCl was investigated by MD simulations, comparing the binding energies of chloride ions bound to the

second halide-binding site in the wild type with the putative site in DbeA ΔCl. The calculated difference in the binding energies between DbeA wt and DbeA ΔCl was 8.7 ± 2.7 kcal mol^{-1}. Binding of a chloride ion to the second chloride-binding site Cl2 was clearly more energetically favourable in the wild-type enzyme than in the double-point mutant. Stopped-flow fluorescence of halide binding to DbeA ΔCl showed only a rapid equilibrium phase (Fig. 3*b* and Supplementary Fig. 3*b*), confirming the absence of the second halide-binding site in this protein. The dissociation constant

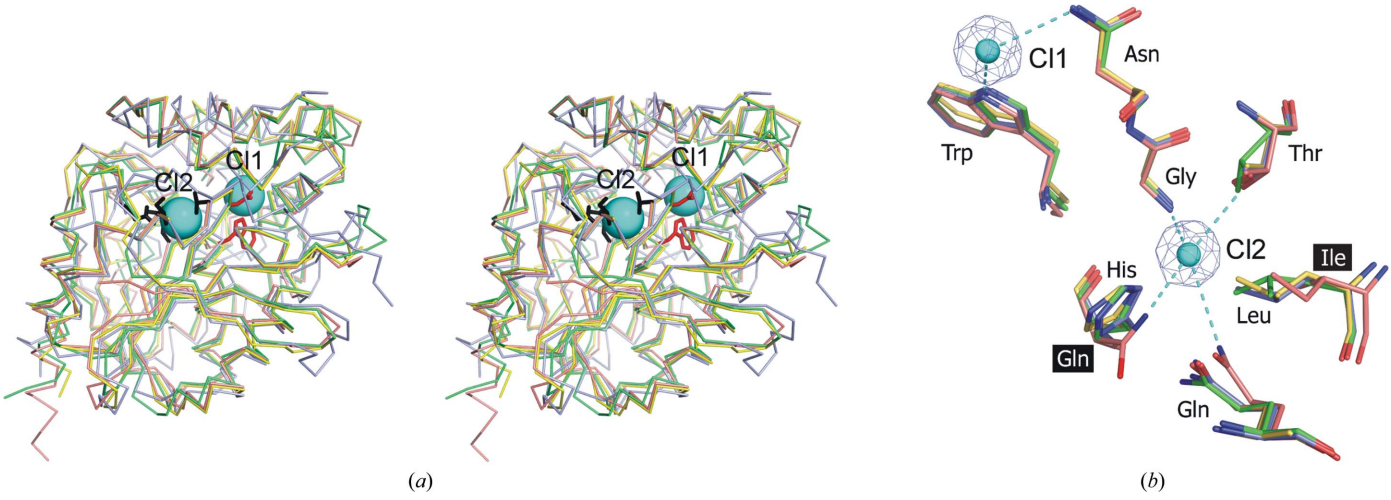

Figure 4
Comparison of the DbeA structure and halide-binding sites with other HLDs. (*a*) Stereoview of the structure of DbeA from *B. elkanii* (red, PDB entry 4k2a) superposed with DhaA from *Rhodococcus* sp. (yellow, PDB entry 1bn6), DmbA from *M. tuberculosis* Rv2579 (blue, PDB entry 2qvb) and LinB from *S. japonicum* UT26 (green, PDB entry 1cv2). Chloride ions bound to DbeA are shown as cyan spheres; halide-binding residues coordinating Cl1 are shown as red sticks; the residues coordinating Cl2 are shown as dark grey sticks. (*b*) Superposition of the halide-binding sites of DbeA (C atoms in pink), DhaA (C atoms in yellow), DmbA (C atoms in light blue) and LinB (C atoms in green). Chloride ions coordinated in DbeA are represented by cyan spheres; the $2F_o - F_c$ electron-density map contoured at 1.5σ is shown in blue.

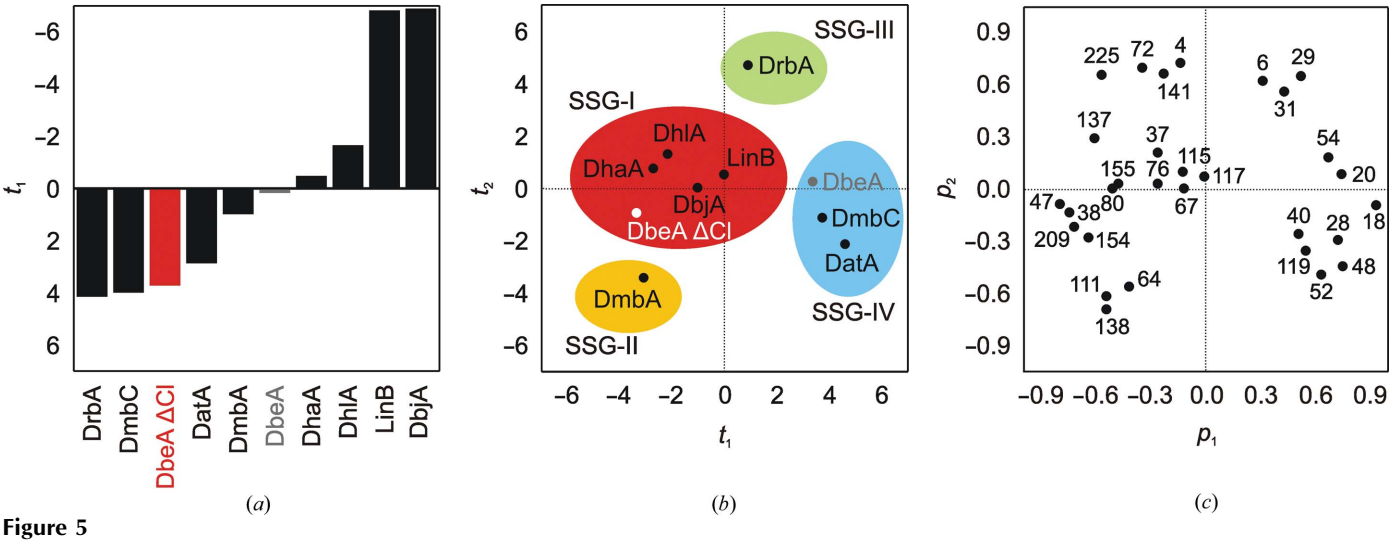

Figure 5
Statistical analyses of the substrate-specificity data. (*a*) The score-contribution plot t_1 from principal component analysis (PCA) with the untransformed data set. The plot shows differences in the overall activities of individual HLDs. The overall activity of DbeA ΔCl is similar to that of the least active enzymes, DrbA and DmbC. The plot explains 56% of the variance in the data set. (*b*) The score plot t_1/t_2 from PCA with the transformed data set. The score plot is a two-dimensional window into multidimensional space, where the objects (enzymes) with similar properties (specificity profiles) are co-located. The t_1/t_2 score plot describing 46% of variance in the data set shows the enzymes clustered in individual substrate-specificity groups (SSGs). Unlike DbeA wt, DbeA ΔCl is positioned in SSG-I, together with LinB, DbjA, DhaA and DhlA. All members of SSG-I possess broad substrate specificity. (*c*) The corresponding loading plot p_1/p_2 from PCA with the transformed data set showing the main substrates for each SSG. Numbering of the substrates is as follows: 1-chlorobutane (4), 1-chlorohexane (6), 1-bromobutane (18), 1-bromohexane (20), 1-iodopropane (28), 1-iodobutane (29), 1-iodohexane (31), 1,2-dichloroethane (37), 1,3-dichloropropane (38), 1,5-dichloropentane (40), 1,2-dibromoethane (47), 1,3-dibromopropane (48), 1-bromo-3-chloropropane (52), 1,3-diiodopropane (54), 2-iodobutane (64), 1,2-dichloropropane (67), 1,2-dibromopropane (72), 2-bromo-1-chloropropane (76), 1,2,3-trichloropropane (80), bis(2-chloroethyl)ether (111), chlorocyclohexane (115), bromocyclohexane (117), (bromomethyl)cyclohexane (119), 1-bromo-2-chloroethane (137), chlorocyclopentane (138), 4-bromobutyronitrile (141), 1,2,3-tribromopropane (154), 1,2-dibromo-3-chloropropane (155), 3-chloro-2 methylpropene (209) and 2,3-dichloropropene (225).

Table 2
Steady-state and pre-steady-state kinetic constants of DbeA wt and DbeA ΔCl with the substrate 1-bromobutane.

$K_{0.5}$ is the concentration of substrate at half maximal velocity, k_{cat} is the catalytic constant, n is the Hill coefficient, K_{si} is the substrate-inhibition constant, k_{obs} is the rate constant for the burst phase of product formation and k_{ss} is the rate constant for the steady-state phase of product formation. All measurements were performed at pH 8.6 and 37°C.

Enzyme	k_{cat} (s^{-1})	$K_{0.5}$ (mM)	n	K_{si} (mM)	k_{obs} (s^{-1})	k_{ss} (s^{-1})
DbeA wt	3.91 ± 0.16†	0.51 ± 0.02†	1.33 ± 0.09†	27.06 ± 3.05†	71 ± 39‡	2.54 ± 0.07‡
DbeA ΔCl	0.038 ± 0.002§	0.011 ± 0.001§	2.11 ± 0.01§	¶	77 ± 15‡	0.063 ± 0.005‡

† Kinetic parameters were calculated using the Hill equation modified by additional terms for substrate inhibition: $(v/V_{lim}) = [S]^n/(K^n + [S]^n\{1+ ([S]/K_{si})\})$. ‡ Kinetic parameters were calculated using the burst equation: $[P]/[E]_0 = A_0[1 - \exp(-k_{obs}t)] + k_{ss}t$. § Kinetic parameters were calculated using the Hill equation: $(v/V_{lim}) = [S]^n/(K^n + [S]^n)$. ¶ Not applicable.

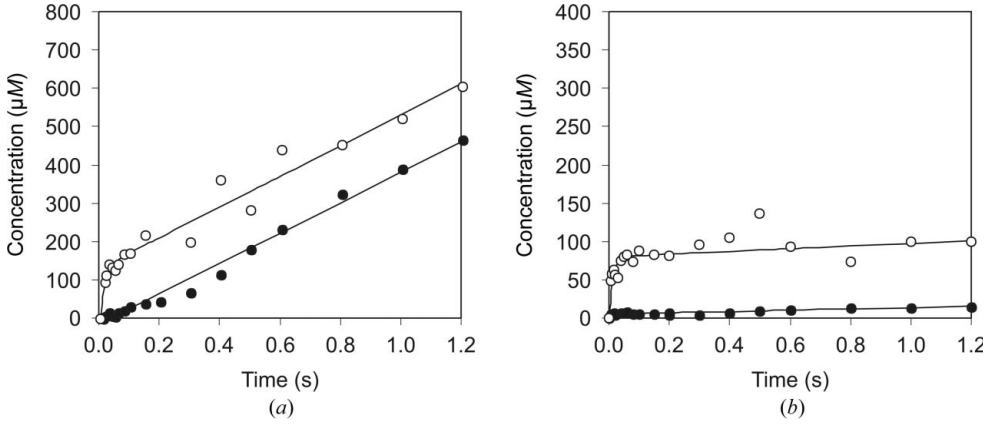

Figure 6
Rapid-quench flow analysis of the burst phase of DbeA wt and DbeA ΔCl reactions. The burst in reaction was monitored upon mixing (*a*) 155 μ*M* DbeA wt with 1400 μ*M* 1-bromobutane and (*b*) 140 μ*M* DbeA ΔCl with 600 μ*M* 1-bromobutane. Solid lines represent the best fits to the bromide ion (empty circles) and 1-butanol (filled circles) kinetic data.

calculated from the dependence of the fluorescence quench amplitude of DbeA ΔCl on chloride concentration was K_d = 2.30 ± 1.00 *M* (Fig. 3*d*).

3.4. Effect of elimination of the second halide-binding site on the substrate specificity of DbeA ΔCl

The specific activity of DbeA ΔCl was assayed with the set of 30 halogenated compounds originally used for characterization of the wild-type enzyme (DbeA wt). DbeA ΔCl exhibited significantly lower activity than DbeA wt with almost all tested compounds (Fig. 5 and Supplementary Table S1). An approximately 40-fold decrease in activity was observed in the case of the iodinated substrates 1-iodobutane and 1,3-diiodopropane and the long-chain chlorinated substrates 1,5-dichloropentane and 1-chlorohexane. Statistical analysis of the transformed activity data set clustered DbeA ΔCl into substrate-specificity group SSG-I (Fig. 5) owing to its reduced preference for iodinated and brominated compounds. In contrast, DbeA wt has been found to cluster into SSG-IV (Koudelakova *et al.*, 2011). The data suggest that elimination of the second halide-binding site dramatically affects the catalytic activity and substrate specificity of the enzyme.

3.5. Effect of elimination of the second halide-binding site on the kinetics of DbeA ΔCl

The catalytic efficiency of the mutant enzyme was assessed by determining the steady-state kinetic constants for 1-bromobutane conversion using isothermal titration calorimetry. DbeA ΔCl exhibited a much lower K_m, as well as a sizeable decrease in k_{cat} (Table 2), suggesting that the low specific activities of DbeA ΔCl observed during substrate screening are owing to a low catalytic rate. Moreover, substrate inhibition was not observed with this variant.

To identify the kinetic steps affected by elimination of the second halide-binding site, transient kinetic experiments were conducted with DbeA wt and DbeA ΔCl using 1-bromobutane as a substrate. Upon rapid mixing of DbeA wt or DbeA ΔCl with excess of substrate, a clear pre-steady-state burst of bromide production was observed (Fig. 6). All steps leading to the formation of halide ion, substrate binding and subsequent cleavage of the carbon–halogen bond are fast and do not limit overall steady-state turnover. On the other hand, only linear formation of the alcohol product with no sign of a burst was observed even in the early transient phase of the reaction (Fig. 6). Since all steps before hydrolysis of the alkyl-enzyme intermediate are fast, the absence of an alcohol burst suggests that the hydrolysis of the alkyl-enzyme intermediate is a rate-determining step for the catalytic conversion of 1-bromobutane. The rate constants calculated for the burst phase of bromide formation (k_{obs}) were similar for both enzymes, suggesting that elimination of the second halide-binding site did not affect the rate of substrate binding or the cleavage of the carbon–halogen bond (Table 2). However, a significant reduction in the rate of the linear steady-state phase (k_{ss}) was observed, indicating that the hydrolytic step of the catalytic cycle was severely affected by the introduced mutations (Table 2).

The catalytic histidine plays an essential role in the hydrolysis of the alkyl-enzyme intermediate by abstraction of the proton from the catalytic water. The pK_a of the catalytic histidine in DbeA wt with and without a chloride anion bound to the second halide-binding site was calculated at constant pH and compared with the pK_a of the catalytic histidine in DbeA ΔCl. The pK_a in DbeA wt (pK_a = 7.1 ± 1.4) without a

chloride anion present was comparable to the pK_a in DbeA ΔCl (pK_a = 7.3 ± 0.5), which lacked the second halide-binding site. In the case of DbeA wt with a chloride anion present, the pK_a of the catalytic histidine increased notably (pK_a = 9.6 ± 0.8), implying that it is a stronger base. It is worth mentioning that these calculations are sensitive to the choice of relative dielectric constant for the protein interior. If the site is more solvated than apparent from the crystal structure, the use of a higher relative dielectric constant would be more appropriate, leading to a smaller difference in pK_a.

3.6. Effect of elimination of the second halide-binding site on the stability of DbeA ΔCl

Proper folding of DbeA ΔCl was verified by CD spectroscopy. No differences between the CD spectra of DbeA wt and its variant were observed (Fig. 7*a*), suggesting that the introduced substitutions have no effect on the secondary structure of DbeA ΔCl. To explore the structural resistance of DbeA wt and DbeA ΔCl towards salts, far-UV CD spectra were measured in the presence of various concentrations of sodium chloride. The secondary structure of each protein was preserved at all tested salt concentrations (Supplementary Fig. S4). At the same time, thermally induced denaturation was tested in the presence and absence of various concentrations of sodium chloride to investigate the effect of the second halide-binding site on the thermal stability of the tested enzymes. The introduced mutations had no effect on the stability of DbeA ΔCl in the absence of salt. Its melting temperature (T_m = 58.0 ± 0.2°C) was almost identical to that of the wild-type enzyme (T_m = 58.5 ± 0.2°C). However, the thermal stability of both enzymes changed significantly in the presence of chloride salts (Fig. 7*b*). The T_m values of DbeA wt increased in a concentration-dependent manner over the whole range of sodium chloride concentrations used. The highest thermostability of DbeA wt (T_m = 66.4 ± 0.1°C) was obtained at the highest tested concentration of sodium chloride (3000 m*M*). In contrast, the T_m values of DbeA ΔCl slightly decreased for sodium chloride concentrations in the range 0–500 m*M* but increased at higher concentrations (1000–1500 m*M*). Increasing the salt concentration further caused a decrease in the thermal stability of DbeA ΔCl. Finally, with a sodium chloride concentration of 3000 m*M*, the stability of DbeA ΔCl was almost comparable with that measured in pure buffer (Fig. 7*b*). The second halide-binding site in DbeA wt appears to be responsible for the higher resistance of this enzyme towards thermally induced denaturation in the presence of a high concentration of chloride salts (1000–3000 m*M*).

4. Discussion

Structural analysis of the newly isolated haloalkane dehalogenase DbeA from *B. elkanii* USDA94 revealed the presence of two halide-binding sites, both fully occupied by chloride anion, buried in the protein core. The first halide-binding site, formed by the two halide-stabilizing residues Asn38 and Trp104, is responsible for stabilization of the halide ion after carbon–halogen bond cleavage. This halide-binding site, which is common to all HLDs, has been found to be occupied by various halide ions in a number of crystal structures: chloride, bromide or iodide ion in DhlA (PDB entries 1b6g, 1edb, 1edd, 2dhd, 2dhe, 1cij, 2eda and 2edc; Verschueren, Kingma *et al.*, 1993; Verschueren, Seljée *et al.*, 1993; Pikkemaat *et al.*, 1999; Ridder *et al.*, 1999), iodide ion in DhaA (PDB entry 1cqw; Newman *et al.*, 1999), chloride or bromide ion in LinB (PDB entries 2g42, 2g4h, 1g5f, 1iz7, 1k5p, 1mj5, 2bfn, 1k63, 1k6e, 1do7 and 1iz8; Marek *et al.*, 2000; Oakley *et al.*, 2002, 2004; Streltsov *et al.*, 2003; Monincová *et al.*, 2007), chloride or bromide ion in DmbA (PDB entries 2qvb, 2o2h and 2o2i; Mazumdar *et al.*, 2008), chloride ion in DbjA (PDB entries 3afi, 3a2n and 3a2m; Prokop *et al.*, 2010). The second chloride-binding site is located approximately 10 Å from the first binding site. This second site is unique to DbeA and has not previously been observed in the crystal structures of related enzymes.

The second halide-binding site of DbeA is buried in the protein core and is lined by five amino-acid residues: Gly37, Thr40, Ile44, Gln102 and Gln274. The same halide-binding motif, G-T-I-Q-Q, has been identified in the sequences of the evolutionarily closely related (sequence identity 56–76%) enzymes DbjA from *B. japonicum* USDA110 (Sato *et al.*, 2005), DmlA from *Mesorhizobium loti* MAFF303099 (Sato *et al.*, 2005), DmhA from *M. huakuii* subsp. *rengei* (unpublished data) and three other putative dehalogenase sequences from *M. ciceri* biovar *biserrulae* WSM1271 (GI:319779915), *Burkholderia* sp. H160 (GI:209502163) and *Chthoniobacter flavus* Ellin428

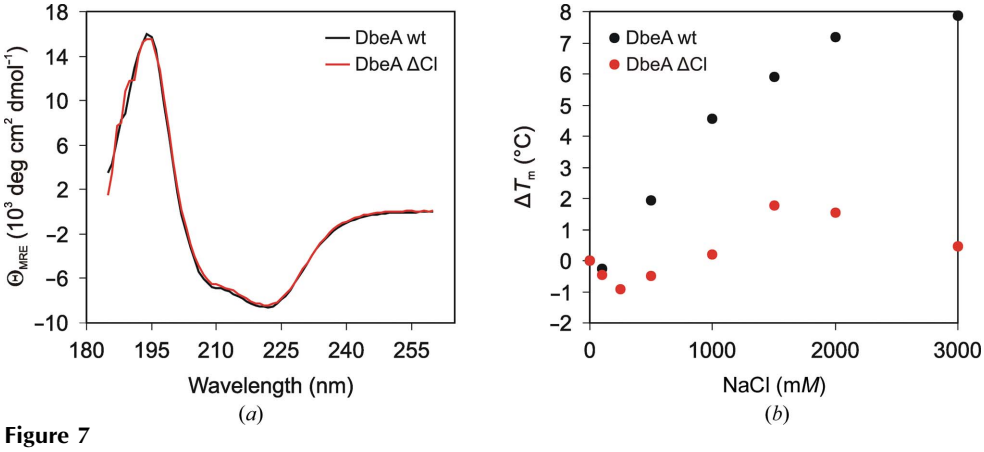

Figure 7
Secondary structure and stability of DbeA wt and DbeA ΔCl in the presence of chloride ions. (*a*) Far-UV CD spectra of DbeA wt and DbeA ΔCl and (*b*) thermal stability of DbeA wt and DbeA ΔCl in the presence of various concentrations of sodium chloride.

(GI:196221892). Among these proteins, the tertiary structure has so far only been solved for DbjA (Sato *et al.*, 2007; Prokop *et al.*, 2010), but the presence of two halide anions in the structure of DbjA was not reported.

The successful removal of the second halide-binding site in the DbeA structure was experimentally confirmed by stopped-flow analysis of chloride binding to DbeA wt and DbeA ΔCl. Elimination of the second halide-binding site dramatically changed the substrate specificity of the enzyme to the extent that the engineered DbeA ΔCl clustered in a different substrate-specificity group, SSG-I, to its parental enzyme, which belonged to SSG-IV. The enzymes in SSG-I are active towards most of the tested substrates, including poorly degradable compounds such as, for example, 1,2-dichloroethane, 1,2-dichloropropane, 1,2,3-trichloropropane and chlorocyclohexane. On the other hand, the enzymes in SSG-IV are more selective for specific halogenated substrates and predominantly exhibit activity towards terminally substituted brominated and iodinated propanes and butanes (Koudelakova *et al.*, 2011). Unlike DbeA wt, DbeA ΔCl was clustered into SSG-I owing to its decreased preference for iodinated and brominated compounds. There have been several previous attempts to modify the substrate specificity of HLDs by engineering their access tunnels and active sites (Chaloupková *et al.*, 2003; Pavlova *et al.*, 2009; Koudelakova *et al.*, 2011), since the architecture and dynamics of these two structural elements are believed to influence the preference of the enzyme for a particular type of substrate (Damborský & Koca, 1999; Marek *et al.*, 2000; Bohác *et al.*, 2002; Otyepka & Damborský, 2002; Kmunícek *et al.*, 2005; Silberstein *et al.*, 2007; Koudelakova *et al.*, 2011). Although changes in the substrate specificity have been achieved by mutagenesis, a switch in the substrate-specificity class has not previously been observed (Koudelakova *et al.*, 2011). In the present study, the marked switch in specificity class by elimination of the second halide-binding site suggests that halide ions buried inside the protein core are an important determinant of the substrate specificity of HLDs.

Elimination of the second halide-binding site from the protein interior considerably altered the thermal stability of DbeA in the presence of halide ions, without affecting its secondary structure. The wild-type enzyme was more stable in the presence of chloride salts than its variant. The melting temperature of DbeA wt increased with increasing concentrations of salt, whereas only small changes in stability were observed for DbeA ΔCl. The lower stabilization of DbeA ΔCl in the presence of chloride ions is consistent with weaker binding of chloride ions to this enzyme, and therefore a smaller binding energy compared with that of DbeA wt. Our data demonstrate the importance of the second halide-binding site for enzyme stability in the presence of salts. Enzyme stabilization by anions bound to the protein surface as well as the protein core is a phenomenon that has been described in the scientific literature (Kohn *et al.*, 1997; Zhang & Cremer, 2006; Tadeo *et al.*, 2007; Ogawa *et al.*, 2010). Investigation of the role of halide ions in shaping the protein architecture revealed that buried halide motifs are generally associated with high protein stability (Zhou *et al.*, 2010). It was shown that the majority of the stabilization energy in halide motifs buried in the protein interior is not owing to electrostatics, but originates from dispersion forces.

Besides protein stability, the halide anions buried in the protein core can affect other properties, such as catalytic activity, solubility, crystallizability and allosteric propensity (Zhou *et al.*, 2010). DbeA wt exhibited substantially higher catalytic activity than DbeA ΔCl. The mutant was classified as belonging to the least active HLDs, such as DrbA and DmbC, in contrast to the parental enzyme, which exhibited an overall activity similar to those of DhaA, DmbA and DhlA (Koudelakova *et al.*, 2011). Pre-steady-state kinetic burst experiments showed that the high activity of DbeA wt is connected with acceleration of the hydrolytic step. The second reaction step of hydrolytic dehalogenation catalyzed by HLDs is initiated by the attack of an activated water molecule on the alkyl-enzyme intermediate. The catalytic histidine serves as a proton carrier and activates the water molecule. We hypothesize based on pK_a calculations that a chloride anion bound in close proximity to the catalytic histidine may increase its basicity and thus may accelerate the nucleophilic addition of water to the alkyl-enzyme intermediate.

Several structures in the Protein Data Bank contain halides in the interior or on the protein surface (Blasiak & Drennan, 2009; Zhou *et al.*, 2010). In the majority of these structures the halide ions are likely to be an experimental artifact (Blasiak & Drennan, 2009). Two buried halide-binding sites have been reported for a few catalysts belonging to different enzyme classes, for example human myelopexidase (EC 1.11.1.7; Fiedler *et al.*, 2000; Blair-Johnson *et al.*, 2001), human testicular angiotensin-converting enzyme (EC 3.4.15.1; Natesh *et al.*, 2003) and photosystem II (EC 1.10.3.9; Murray *et al.*, 2008; Kawakami *et al.*, 2009).

In human myelopexidase, halides bind to distal and proximal cavities within the catalytic site. The chloride ion bound to the distal cavity serves as a reaction co-substrate and participates in the production of hypochlorous acid. Binding of the second ion to the proximal cavity allows the distal pocket to generate a low-spin haem iron. When hypochlorous acid is generated, the second ion bound to the proximal cavity moves to replace the first one. This action is accompanied by the expulsion of a hypochlorous acid molecule. The chloride ions in human myelopexidase serve as both a substrate and inhibitor and modulate the haem microenvironment (Fiedler *et al.*, 2000; Blair-Johnson *et al.*, 2001; Furtmüller *et al.*, 2006; Proteasa *et al.*, 2007; Blasiak & Drennan, 2009).

In angiotensin-converting enzyme, two buried chloride ions have been found that are separated by 20.3 Å. The two chloride ions are located 20.7 and 10.4 Å away from the zinc ion of the active site. The first chloride ion is bound to two arginines, tryptophan and water, and is surrounded by a hydrophobic shell of four tryptophan residues. The first chloride is important for stabilization of the substrate in the binding groove, while the second halide ion serves as an ionic 'switch' and activates the enzyme by positioning the amino-acid residues for stabilization of the enzyme–substrate

complex (Natesh *et al.*, 2003; Tzakos *et al.*, 2003; Moiseeva *et al.*, 2005; Pokhrel *et al.*, 2011).

Two chloride-binding sites have also been identified in two of the three crystal structures of photosystem II (Murray *et al.*, 2008; Guskov *et al.*, 2009; Kawakami *et al.*, 2009; Pokhrel *et al.*, 2011). The two chloride ions are separated by approximately 14 Å and are located approximately 6–7 Å from the metal ion of the enzyme active site. Activation of photosystem II by chloride binding to site 1 involves a structural change that results in an optimal framework of amino acids around the oxygen-evolving complex, as well as fine-tuning of the pK_a of the residues involved in proton transport. A chloride ion may also be present at the lower affinity site 2, which together with the chloride at site 1 is required for maintaining the coordination structure of the oxygen-evolving complex and opening of the proton channel (Murray *et al.*, 2008; Pokhrel *et al.*, 2011).

In summary, we show that the newly isolated haloalkane dehalogenase DbeA from *B. elkanii* USDA94 possesses two fully occupied chloride-binding sites buried in the protein interior. The first halide-binding site Cl1 is common to all members of the haloalkane dehalogenase family, whereas the second halide-binding Cl2 site was observed for the first time in DbeA. Elimination of the second halide-binding site by introduction of the double point mutation I44L+Q102H (i) dramatically changed the substrate specificity, (ii) decreased the catalytic activity by an order of magnitude, (iii) eliminated the substrate inhibition with 1-bromobutane and (iv) reduced the stability of the enzyme in the presence of high concentrations of chloride salts by 8°C. Switching of the substrate-specificity class by mutagenesis is demonstrated for the first time for this enzyme family.

5. Related literature

The following references are cited in the Supporting Information for this article: Chaloupková *et al.* (2003), Koudelakova *et al.* (2011), Monincová (2007) and Schindler *et al.* (1999).

This work was supported by the Grant Agency of the Czech Republic (P207/12/0775), the Academy of Sciences of the Czech Republic (AV0Z40550506 and AV0Z50520514), the Ministry of Education of the Czech Republic (LO1214) and the Grants-in-Aid for Scientific Research from the Ministry of Education, Culture, Sports, Science, and Technology, and the Ministry of Agriculture, Forestry, and Fisheries of Japan. MetaCentrum is acknowledged for providing access to computing facilities supported by the Ministry of Education of the Czech Republic (LM2010005). We would like to express thanks to our technicians Monika Pokorna, Zuzana Martinkova and Hana Moskalikova (Masaryk University) for help with enzyme preparation and rapid-quench flow experiments and to Dr Mihaly Kovacs (Eötvös University) for useful advice on interpretation of the transient kinetic data.

References

Blair-Johnson, M., Fiedler, T. & Fenna, R. (2001). *Biochemistry*, **40**, 13990–13997.
Blasiak, L. C. & Drennan, C. L. (2009). *Acc. Chem. Res.* **42**, 147–155.
Bohác, M., Nagata, Y., Prokop, Z., Prokop, M., Monincová, M., Tsuda, M., Koca, J. & Damborský, J. (2002). *Biochemistry*, **41**, 14272–14280.
Bosma, T., Pikkemaat, M. G., Kingma, J., Dijk, J. & Janssen, D. B. (2003). *Biochemistry*, **42**, 8047–8053.
Case, D. A. *et al.* (2010). *Amber*11. University of California, San Francisco.
Chaloupková, R., Sýkorová, J., Prokop, Z., Jesenská, A., Monincová, M., Pavlová, M., Tsuda, M., Nagata, Y. & Damborský, J. (2003). *J. Biol. Chem.* **278**, 52622–52628.
Chan, W. Y., Wong, M., Guthrie, J., Savchenko, A. V., Yakunin, A. F., Pai, E. F. & Edwards, E. A. (2010). *Microb. Biotechnol.* **3**, 107–120.
Chen, V. B., Arendall, W. B., Headd, J. J., Keedy, D. A., Immormino, R. M., Kapral, G. J., Murray, L. W., Richardson, J. S. & Richardson, D. C. (2010). *Acta Cryst.* D**66**, 12–21.
Chovancová, E., Kosinski, J., Bujnicki, J. M. & Damborský, J. (2007). *Proteins*, **67**, 305–316.
Damborsky, J., Chaloupkova, R., Pavlova, M., Chovancova, E. & Brezovsky, J. (2010). *Handbook of Hydrocarbon and Lipid Microbiology*, edited by K. N. Timmis, pp. 1081–1098. Berlin/Heidelberg: Springer-Verlag.
Damborský, J. & Koca, J. (1999). *Protein Eng.* **12**, 989–998.
Damborský, J., Rorije, E., Jesenská, A., Nagata, Y., Klopman, G. & Peijnenburg, W. J. (2001). *Environ. Toxicol. Chem.* **20**, 2681–2689.
Darden, T., York, D. & Pedersen, L. (1993). *J. Chem. Phys.* **98**, 10089.
Drienovska, I., Chovancova, E., Koudelakova, T., Damborsky, J. & Chaloupkova, R. (2012). *Appl. Environ. Microbiol.* **78**, 4995–4998.
Emsley, P. & Cowtan, K. (2004). *Acta Cryst.* D**60**, 2126–2132.
Fasman, G. D. (1996). *Circular Dichroism and the Conformational Analysis of Biomolecules.* New York: Plenum Press.
Fiedler, T. J., Davey, C. A. & Fenna, R. E. (2000). *J. Biol. Chem.* **275**, 11964–11971.
Franken, S. M., Rozeboom, H. J., Kalk, K. H. & Dijkstra, B. W. (1991). *EMBO J.* **10**, 1297–1302.
Furtmüller, P. G., Zederbauer, M., Jantschko, W., Helm, J., Bogner, M., Jakopitsch, C. & Obinger, C. (2006). *Arch. Biochem. Biophys.* **445**, 199–213.
Gehret, J. J., Gu, L., Geders, T. W., Brown, W. C., Gerwick, L., Gerwick, W. H., Sherman, D. H. & Smith, J. L. (2012). *Protein Sci.* **21**, 239–248.
Gordon, J. C., Myers, J. B., Folta, T., Shoja, V., Heath, L. S. & Onufriev, A. (2005). *Nucleic Acids Res.* **33**, W368–W371.
Guskov, A., Kern, J., Gabdulkhakov, A., Broser, M., Zouni, A. & Saenger, W. (2009). *Nature Struct. Mol. Biol.* **16**, 334–342.
Hasan, K., Fortova, A., Koudelakova, T., Chaloupkova, R., Ishitsuka, M., Nagata, Y., Damborsky, J. & Prokop, Z. (2011). *Appl. Environ. Microbiol.* **77**, 1881–1884.
Hasan, K., Gora, A., Brezovsky, J., Chaloupkova, R., Moskalikova, H., Fortova, A., Nagata, Y., Damborsky, J. & Prokop, Z. (2013). *FEBS J.* **280**, 3149–3159.
Hesseler, M., Bogdanović, X., Hidalgo, A., Berenguer, J., Palm, G. J., Hinrichs, W. & Bornscheuer, U. T. (2011). *Appl. Microbiol. Biotechnol.* **91**, 1049–1060.
Holmquist, M. (2000). *Curr. Protein Pept. Sci.* **1**, 209–235.
Hornak, V., Abel, R., Okur, A., Strockbine, B., Roitberg, A. & Simmerling, C. (2006). *Proteins*, **65**, 712–725.
Humphrey, W., Dalke, A. & Schulten, K. (1996). *J. Mol. Graph.* **14**, 33–38.
Iwasaki, I., Utsumi, S. & Ozawa, T. (1952). *Bull. Chem. Soc. Jpn*, **25**, 226.
Janssen, D. B. (2004). *Curr. Opin. Chem. Biol.* **8**, 150–159.
Jesenská, A., Bartos, M., Czerneková, V., Rychlík, I., Pavlík, I. & Damborský, J. (2002). *Appl. Environ. Microbiol.* **68**, 3724–3730.
Jesenská, A., Monincová, M., Koudeláková, T., Hasan, K., Chaloupková, R., Prokop, Z., Geerlof, A. & Damborsky, J. (2009). *Appl. Environ. Microbiol.* **75**, 5157–5160.

Jesenská, A., Pavlová, M., Strouhal, M., Chaloupková, R., Tesínská, I., Monincová, M., Prokop, Z., Bartos, M., Pavlík, I., Rychlík, I., Möbius, P., Nagata, Y. & Damborsky, J. (2005). *Appl. Environ. Microbiol.* **71**, 6736–6745.

Jones, S. & Thornton, J. M. (1996). *Proc. Natl Acad. Sci. USA*, **93**, 13–20.

Jorgensen, W. L., Chandrasekhar, J., Madura, J. D., Impey, R. W. & Klein, M. L. (1983). *J. Chem. Phys.* **79**, 926.

Kawakami, K., Umena, Y., Kamiya, N. & Shen, J.-R. (2009). *Proc. Natl Acad. Sci. USA*, **106**, 8567–8572.

Keuning, S., Janssen, D. B. & Witholt, B. (1985). *J. Bacteriol.* **163**, 635–639.

Kmunícek, J., Hynková, K., Jedlicka, T., Nagata, Y., Negri, A., Gago, F., Wade, R. C. & Damborský, J. (2005). *Biochemistry*, **44**, 3390–3401.

Kohn, W. D., Kay, C. M. & Hodges, R. S. (1997). *J. Mol. Biol.* **267**, 1039–1052.

Koudelakova, T., Chovancova, E., Brezovsky, J., Monincova, M., Fortova, A., Jarkovsky, J. & Damborsky, J. (2011). *Biochem. J.* **435**, 345–354.

Krissinel, E. & Henrick, K. (2005). *CompLife 2005*, edited by M. R. Berthold, R. Glen, K. Diederichs, O. Kohlbacher & I. Fischer, pp. 163–174. Berlin/Heidelberg: Springer-Verlag.

Krissinel, E. & Henrick, K. (2007). *J. Mol. Biol.* **372**, 774–797.

Krooshof, G. H., Ridder, I. S., Tepper, A. W., Vos, G. J., Rozeboom, H. J., Kalk, K. H., Dijkstra, B. W. & Janssen, D. B. (1998). *Biochemistry*, **37**, 15013–15023.

Kulakova, A. N., Larkin, M. J. & Kulakov, L. A. (1997). *Microbiology*, **143**, 109–115.

Marek, J., Vévodová, J., Smatanová, I. K., Nagata, Y., Svensson, L. A., Newman, J., Takagi, M. & Damborský, J. (2000). *Biochemistry*, **39**, 14082–14086.

Mazumdar, P. A., Hulecki, J. C., Cherney, M. M., Garen, C. R. & James, M. N. G. (2008). *Biochim. Biophys. Acta*, **1784**, 351–362.

Minor, W., Cymborowski, M., Otwinowski, Z. & Chruszcz, M. (2006). *Acta Cryst.* D**62**, 859–866.

Moiseeva, N. A., Binevski, P. V., Baskin, I. I., Palyulin, V. A. & Kost, O. A. (2005). *Biochemistry*, **70**, 1167–1172.

Mongan, J., Case, D. A. & McCammon, J. A. (2004). *J. Comput. Chem.* **25**, 2038–2048.

Monincová, M. (2007). PhD thesis. Masaryk University, Czech Republic.

Monincová, M., Prokop, Z., Vévodová, J., Nagata, Y. & Damborsky, J. (2007). *Appl. Environ. Microbiol.* **73**, 2005–2008.

Mueller, U., Darowski, N., Fuchs, M. R., Förster, R., Hellmig, M., Paithankar, K. S., Pühringer, S., Steffien, M., Zocher, G. & Weiss, M. S. (2012). *J. Synchrotron Rad.* **19**, 442–449.

Murray, J. W., Maghlaoui, K., Kargul, J., Ishida, N., Lai, T.-L. L., Rutherford, A. W., Sugiura, M., Boussac, A. & Barber, J. (2008). *Energy Environ. Sci.* **1**, 161–168.

Murshudov, G. N., Skubák, P., Lebedev, A. A., Pannu, N. S., Steiner, R. A., Nicholls, R. A., Winn, M. D., Long, F. & Vagin, A. A. (2011). *Acta Cryst.* D**67**, 355–367.

Nagata, Y., Hynková, K., Damborský, J. & Takagi, M. (1999). *Protein Expr. Purif.* **17**, 299–304.

Nardini, M. & Dijkstra, B. W. (1999). *Curr. Opin. Struct. Biol.* **9**, 732–737.

Natesh, R., Schwager, S. L. U., Sturrock, E. D. & Acharya, K. R. (2003). *Nature (London)*, **421**, 551–554.

Newman, J., Peat, T. S., Richard, R., Kan, L., Swanson, P. E., Affholter, J. A., Holmes, I. H., Schindler, J. F., Unkefer, C. J. & Terwilliger, T. C. (1999). *Biochemistry*, **38**, 16105–16114.

Oakley, A. J., Klvana, M., Otyepka, M., Nagata, Y., Wilce, M. C. J. & Damborský, J. (2004). *Biochemistry*, **43**, 870–878.

Oakley, A. J., Prokop, Z., Bohác, M., Kmunícek, J., Jedlicka, T., Monincová, M., Kutá-Smatanová, I., Nagata, Y., Damborský, J. & Wilce, M. C. J. (2002). *Biochemistry*, **41**, 4847–4855.

Ogawa, H., Qiu, Y., Philo, J. S., Arakawa, T., Ogata, C. M. & Misono, K. S. (2010). *Protein Sci.* **19**, 544–557.

Ollis, D. L., Cheah, E., Cygler, M., Dijkstra, B., Frolow, F., Franken, S. M., Harel, M., Remington, S. J., Silman, I., Schrag, J., Sussman, J. L., Verschueren, K. H. G. & Goldman, A. (1992). *Protein Eng.* **5**, 197–211.

Onufriev, A., Bashford, D. & Case, D. A. (2004). *Proteins*, **55**, 383–394.

Otyepka, M. & Damborský, J. (2002). *Protein Sci.* **11**, 1206–1217.

Pavlova, M., Klvana, M., Prokop, Z., Chaloupkova, R., Banas, P., Otyepka, M., Wade, R. C., Tsuda, M., Nagata, Y. & Damborsky, J. (2009). *Nature Chem. Biol.* **5**, 727–733.

Pikkemaat, M. G., Ridder, I. S., Rozeboom, H. J., Kalk, K. H., Dijkstra, B. W. & Janssen, D. B. (1999). *Biochemistry*, **38**, 12052–12061.

Pokhrel, R., McConnell, I. L. & Brudvig, G. W. (2011). *Biochemistry*, **50**, 2725–2734.

Prokop, Z., Monincová, M., Chaloupková, R., Klvana, M., Nagata, Y., Janssen, D. B. & Damborský, J. (2003). *J. Biol. Chem.* **278**, 45094–45100.

Prokop, Z., Sato, Y., Brezovsky, J., Mozga, T., Chaloupkova, R., Koudelakova, T., Jerabek, P., Stepankova, V., Natsume, R., van Leeuwen, J. G. E., Janssen, D. B., Florian, J., Nagata, Y., Senda, T. & Damborsky, J. (2010). *Angew. Chem. Int. Ed. Engl.* **49**, 6111–6115.

Proteasa, G., Tahboub, Y. R., Galijasevic, S., Raushel, F. M. & Abu-Soud, H. M. (2007). *Biochemistry*, **46**, 398–405.

Prudnikova, T., Mozga, T., Rezacova, P., Chaloupkova, R., Sato, Y., Nagata, Y., Brynda, J., Kuty, M., Damborsky, J. & Kuta Smatanova, I. (2009). *Acta Cryst.* F**65**, 353–356.

Ridder, I. S., Rozeboom, H. J. & Dijkstra, B. W. (1999). *Acta Cryst.* D**55**, 1273–1290.

Ryckaert, J.-P., Ciccotti, G. & Berendsen, H. J. (1977). *J. Comput. Phys.* **23**, 327–341.

Sato, Y., Monincová, M., Chaloupková, R., Prokop, Z., Ohtsubo, Y., Minamisawa, K., Tsuda, M., Damborsky, J. & Nagata, Y. (2005). *Appl. Environ. Microbiol.* **71**, 4372–4379.

Sato, Y., Natsume, R., Tsuda, M., Damborsky, J., Nagata, Y. & Senda, T. (2007). *Acta Cryst.* F**63**, 294–296.

Schanstra, J. P., Kingma, J. & Janssen, D. B. (1996). *J. Biol. Chem.* **271**, 14747–14753.

Schindler, J. F., Naranjo, P. A., Honaberger, D. A., Chang, C.-H., Brainard, J. R., Vanderberg, L. A. & Unkefer, C. J. (1999). *Biochemistry*, **38**, 5772–5778.

Silberstein, M., Damborsky, J. & Vajda, S. (2007). *Biochemistry*, **46**, 9239–9249.

Still, W. C., Tempczyk, A., Hawley, R. C. & Hendrickson, T. (1990). *J. Am. Chem. Soc.* **112**, 6127–6129.

Streltsov, V. A., Prokop, Z., Damborský, J., Nagata, Y., Oakley, A. & Wilce, M. C. J. (2003). *Biochemistry*, **42**, 10104–10112.

Tadeo, X., Pons, M. & Millet, O. (2007). *Biochemistry*, **46**, 917–923.

Tzakos, A. G., Galanis, A. S., Spyroulias, G. A., Cordopatis, P., Manessi-Zoupa, E. & Gerothanassis, I. P. (2003). *Protein Eng.* **16**, 993–1003.

Vagin, A. & Teplyakov, A. (2010). *Acta Cryst.* D**66**, 22–25.

Verschueren, K. H., Kingma, J., Rozeboom, H. J., Kalk, K. H., Janssen, D. B. & Dijkstra, B. W. (1993). *Biochemistry*, **32**, 9031–9037.

Verschueren, K. H., Seljée, F., Rozeboom, H. J., Kalk, K. H. & Dijkstra, B. W. (1993). *Nature (London)*, **363**, 693–698.

Winn, M. D., Isupov, M. N. & Murshudov, G. N. (2001). *Acta Cryst.* D**57**, 122–133.

Winn, M. D. *et al.* (2011). *Acta Cryst.* D**67**, 235–242.

Wold, S., Esbensen, K. & Geladi, P. (1987). *Chemometr. Intell. Lab. Syst.* **2**, 37–52.

Zhang, Y. & Cremer, P. S. (2006). *Curr. Opin. Chem. Biol.* **10**, 658–663.

Zhou, P., Tian, F., Zou, J., Ren, Y., Liu, X. & Shang, Z. (2010). *J. Phys. Chem. B*, **114**, 15673–15686.